On Investigating the Hydrodynamic Field for Jets with and without Installation Effects

Hasan Kamliya Jawahar* and Mahdi Azarpeyvand†,
Department of Aerospace Engineering, University of Bristol, Bristol, United Kingdom, BS8 1TR

Near-field hydrodynamic and acoustic characteristics of an unheated subsonic jet with chevron nozzles were investigated experimentally with and without jet installation effects. Near-field pressure fluctuations were acquired for Mach numbers ranging from 0.3 to 0.9 for four different types of chevron nozzles in an anechoic jet facility at the University of Bristol. The measurements were carried out on an axial microphone array traversed in the radial direction and placed close to the jet. The tests were performed for several plate heights from the nozzle to investigate the effect of plate distance from the jet. The results are presented for sound pressure level and overall sound pressure level for several radial locations. Further analyses were carried out by decomposing the near-field pressure into hydrodynamic and acoustic components. The investigation clearly shows the effect of jet installation on the hydrodynamic and acoustic fields. Auto-correlation and cross-correlation analysis was also carried out for the near-field pressure fluctuations. The convective velocity of the flow is reduced by the use of chevrons. The use of chevron nozzles changes the acoustic pressure in the near-field region thereby shifting the dominant noise source towards the nozzle exit for both the installed and isolated configurations.

I. Introduction

NOISE generated by high-speed propulsive jet engines has remained a challenging fluid dynamics problem since the dawn of jet aircraft. Jet noise forms a major part of the overall aircraft noise, scaling with the jet flow velocity at the nozzle exit. The introduction of high-bypass engines in the 1960s has resulted in improved overall efficiency and reduced noise, especially at take-off (full engine power) conditions due to relatively lower exhaust flow velocity. Several studies have shown that the jet-installation noise with characteristic low and mid-frequency amplifications is dominant at flight regimes such as take-off and approach as deployed high-lift devices are positioned closer to the jet plume.

Several noise reduction technologies have been developed to mitigate the jet installation noise effects [1–12]. From these investigations, it is known that the installation affects jet noise by both modifying the jet turbulence and leading to hydrodynamic wave scattering by the trailing edge of the wing flap. One of the popular noise reduction technologies has been chevron nozzles, which were introduced to enhance the large scale mixing thereby decreasing the coherence of the effective noise sources in the jet [13]. The chevrons are often azimuthally uniform and are triangular in shape. Parameters of the chevron nozzles such as the number of chevrons, their length, and penetration angle strongly affect their noise reduction capabilities as shown by Bridges and Brown [13].

Mengle *et al*. [14] used azimuthally varying chevron nozzles to reduce the Jet-Surface-Interaction noise. These chevrons induce streamwise vorticity into the shear layer resulting in enhanced mixing and reduced jet plume length. Azimuthally varying chevron nozzles showed a noise reduction of up to 2.6 dB and performed better in comparison with the uniformly distributed chevrons, which can be explained by further suppression of the axisymmetric mode of the jet noise sources in comparison with axisymmetric jets. For Jet-Flap-Interaction noise, the source localisation results based on beam-forming also showed that the dominant trailing-edge source could be reduced by the chevron effect on the jet turbulence. Kamliya *et al.* [15] in a recent experimental and computational study showed the noise reduction capabilities of chevron for jet installation effect. The study showed that breakage of large scale structures by the use of chevron results in the reduction of jet installation noise. Overall, it has been well established in the literature that chevron nozzles can reduce peak jet noise by improving the mixing and shortening of the potential core. Although chevron nozzles seem to be an attractive solution to the problem of jet noise, experimental investigation on the effect of chevron on the jet installation effect is yet to be characterised.

In the present paper, an experimental study has been carried out for a subsonic jet at the proximity of a flat plate for four different types of chevron nozzles and various plate positions. The experimental measurements were carried out

*Research Associate, hasan.kj@bristol.ac.uk
†Professor in Aerodynamics and Aeroacoustics, m.azarpeyvand@bristol.ac.uk

using near-field array measurements for a range of plate positions and Mach numbers for both the isolated and installed configurations. This paper presents an in-depth comparative analysis of isolated and installed jets with and without chevrons. The results are presented in terms of differences between the isolated and installed jets, and round and chevron jets. The results are presented for sound pressure levels, overall sound pressure levels, auto-correlation, and cross-correlation to better understand the noise reduction capabilities of the chevron nozzle for installed configuration.

II. Experimental setup

The experiments were conducted in Bristol Jet Aeroacoustic Research Facility (B-JARF) at the University of Bristol [15–19]. The flow in B-JARF is silenced using three different in-line-silencers to create a clean quiet flow down to a jet exit Mach number of M = 0.3 as shown in Fig. 1. There are two small silencers which have a diameter of 0.3 m and a height of 1.5 m each which are placed right after the control valve outside the anechoic chamber. A larger plenum combined silencer with a diameter of 0.457 m and a height of 1.9 m is placed inside the chamber where the flow exit into the chamber and nozzles are mounted. The silencers were equipped with perforated tubes for the flow with the remaining area packed with glass wool. The anechoic chamber where the tests were carried out has dimensions of 7.9 m in length, 5.0 m in width, and 4.6 m in height, including the surrounding acoustic walls [20].

A total of five nozzles were tested, firstly, a round convergent nozzle (SMC 000) and four chevron nozzles (SMC 001, SMC 002, SMC 003, and SMC 004) as shown in Fig. 2. The geometry of the chevron nozzles were acquired from a detailed study carried out by Bridges and Brown [13]. The nozzles tested at BJARF were a down-scaled version of the nozzles used by Bridges and Brown [13], corresponding to an exit diameter of $D = 16.9333$ mm for the SMC 000 round convergent nozzle. The tests were carried out for a wide range of subsonic flows with acoustic Mach numbers ranging from $M = 0.3 - 0.9$. The jet-plate arrangement used in the present experiment is shown in Fig. 4. The flat plate used to study the installation effect was made from a 2 mm thick aluminium and was chamfered to have a sharp trailing edge. The plate was equipped with aluminium spars to increase its rigidity. The plate had a total length of 10D and a total span of 24D to avoid side-edge scattering. The flat plate was mounted on an automated traverse system with the capability to move in the radial direction. As shown in Fig. 4 the tests were carried out for a flat-plate length $L = 6.5D$ and a plate height $h = 2D$ radially away from the jet centre-line. Several plate heights were tested and for the sake of brevity, only the results for plate height $h = 2D$ are presented. The plate extends $3.5D$ upstream from the nozzle exit to avoid scattering effects at the trailing edge. It is noteworthy that the plate is placed in the linear hydrodynamic region, where the pressure decays exponentially with increasing radial distance. Near-field pressure fluctuations were acquired using 1/4-inch GRAS-40PL microphone that has a corrected flat frequency response at frequencies from 10Hz to 20 kHz with a dynamic range of 150 dB. A linear array of 10 microphones placed at a distance of $2D$ away from each other, moved to 12 different locations radially away from the nozzle using a traverse were used for this purpose (see Figs. 3 and 4). The data were acquired using a National Instrument PXIe-4499 for $t = 24$ s at a sampling frequency of $f = 2^{17}$Hz. The sound pressure level (SPL) spectrum can then be calculated from $SPL = 20 \cdot log_{10}\,(p_{rms}/p_{ref})$, where p_{rms} is the root-mean-square of the acoustic pressure and $p_{ref} = 20\ \mu$Pa is the reference pressure.

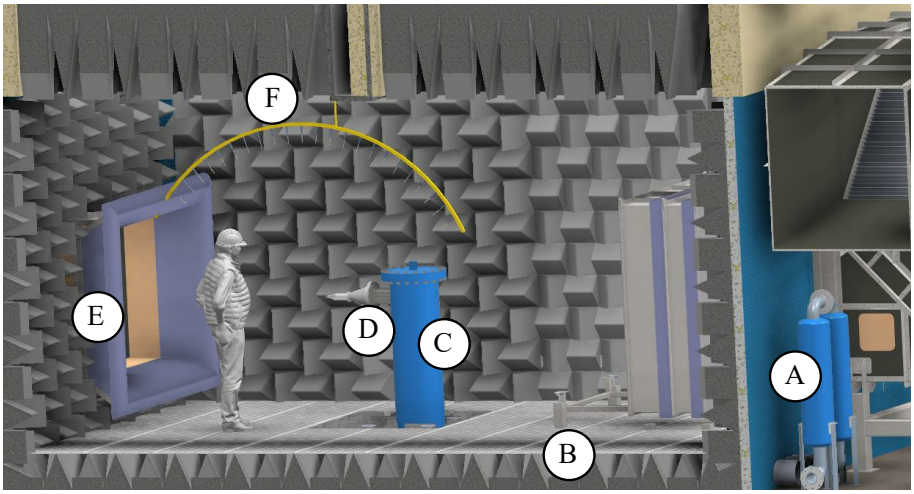

Fig. 1. Side view of the aeroacoustic facility including the silencers: (A) First and second silencer, (B) Connecting underground pipe, (C) Third large silencer, (D) Contraction for the jet nozzle, (E) Collector, and (F) Far-field microphone array.

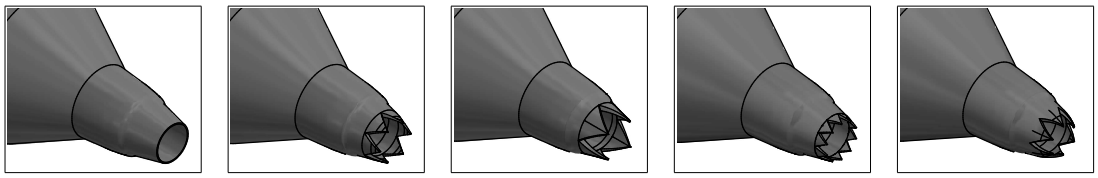

Fig. 2. Schematic of the various nozzle configurations used in the present study.

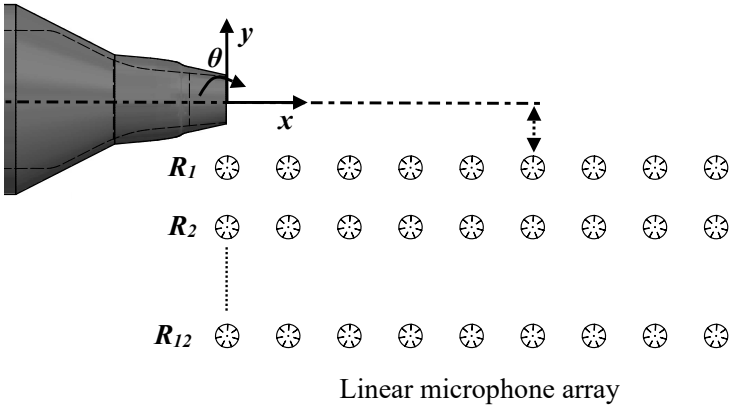

Fig. 3. Schematic of the experimental setup with the position of the near-field microphones used in the present study for the isolated jet.

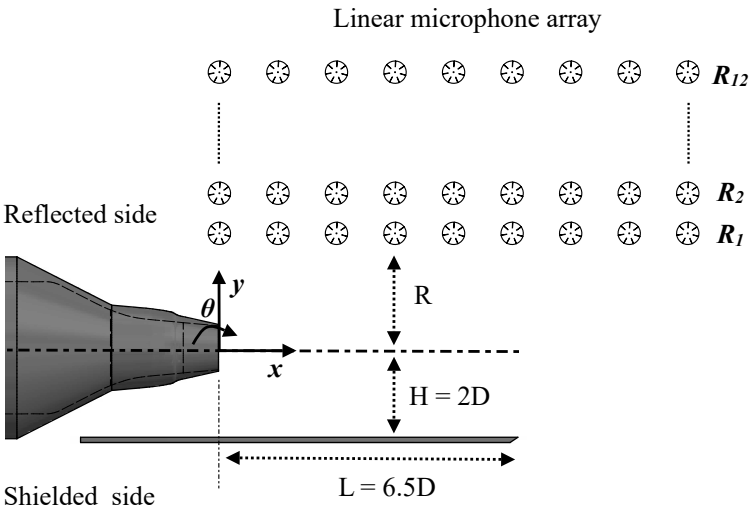

Fig. 4. Schematic of the experimental setup with the position of the near-field microphones used in the present study for the installed jet.

III. Results and Discussion

A. OASPL investigation

Although the nozzles were tested for several plate distances and a wide range of Mach numbers, the results are presented for a plate distance of $h/D = 2$ and acoustic Mach number M=0.5 for the sake of brevity. It is important to note that the BJARF facility has been thoroughly validated in previous studies [15–18]. In order to provide an overview of the near-field characteristics of the tested nozzles, the overall sound pressure level (OASPL) of the near-field microphone array for axial microphones $x/D = 0 - 18$ measured at a distance of $R/D = 3$ is presented in Fig. 5. OASPL for the isolated configuration in Fig. 5 shows notable noise increase for all chevron nozzles at locations $x/D = 0 - 5$. Specifically, SMC002 configuration shows high-pressure levels well past the potential core to $x/D = 5 - 12$. Making a comparison SMC006 configuration shows a notable reduction in the pressure levels past $x/D > 5$. The remaining chevron nozzles show a very minimal reduction past $x/D > 5$. In the case of installed configuration, the increase in pressure level close to the nozzle is contained within $x/D = 4$ for all the tested chevron nozzles. In the case of SMC002, the increase in pressure levels only up to $X/D = 8$ which is a reduction of up to 4D compared to its respective isolated configuration. Interestingly, SMC006 shows a substantial reduction in the near-field pressure levels past $x/D = 6$, whereas the other chevron nozzles do not show any reduction in the turbulence mixing region.

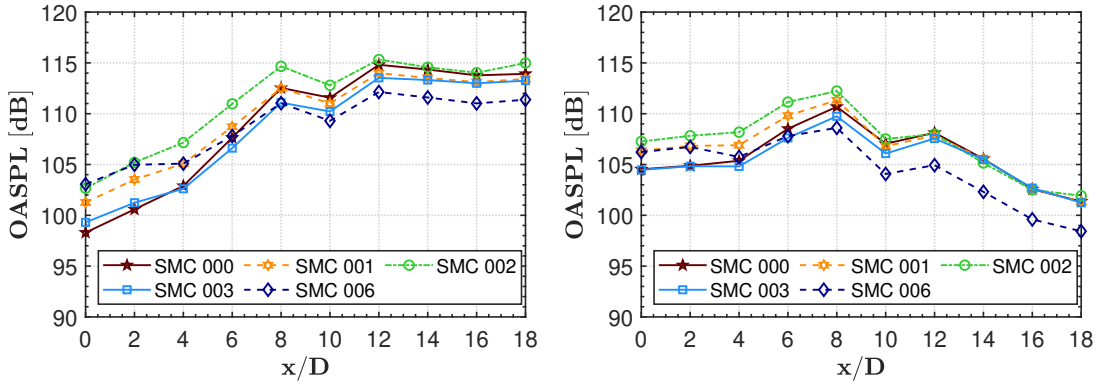

a) Isolated, M = 0.5 b) Installed, M = 0.5

Fig. 5. Overall sound pressure level at radial position $R/D = 3$ at several axial locations $x/D = 0 - 18$ for acoustic Mach number M = 0.5 for both isolated and installed jets with a plate distance of $h/D = 2$.

Overall comparison of the near-field pressure fluctuation can be easily visualised and interpreted through contour maps of the Overall sound pressure level (OASPL). The OASPL calculated for a matrix comprising of several measurement points between $R/D = 0 - 12$ in the radial direction and $x/D = 0 - 18$ in the axial direction is presented in Fig. 6. The OASPL was resolved for a frequency range from $St = 0.01 - 2$. The difference in OASPL between installed and isolated configuration for SMC000 and SMC006 nozzles are presented in Fig. 6a and 6b, respectively. The positive regions of the OASPL contours are contributed by the installed configuration and negative regions are contributed by the isolated configuration. From the results, it is clear that the isolated configuration has high overall pressure levels in the turbulent mixing regions $x/D = 10 - 15$ with an increase of up to 7 dB for SMC000 (shown as negative values in the colour map). SMC006 isolated follows a similar trend but an increase of only 4 dB is observed. When considering the effects of installation for SMC000, it is dominant at radial locations $R/D > 4$ at axial locations $x/D < 4$ with levels up to 6.5 dB. Whereas, in the case of SMC006 the increase in pressure levels is only 4.5 dB and is dominant at radial locations $R/D > 6$ at axial locations $x/D < 4$. These results demonstrate the installation noise reduction capability of the nozzles compared to their respective isolated cases.

The difference in OASPL between SMC000 and SMC006 for isolated and installed configurations are presented in Fig. 6c and 6d, respectively. From the results, the positive regions of the OASPL are contributed by SMC000 and the negative regions are contributed by SMC006. It is clear that SMC006 isolated has high noise levels on the sideline of the nozzle extending radially $R/D = 0 - 12$ at axial locations $x/D < 4$ with high values at the vicinity of the jet exit. In the case of SMC000, high pressure levels are observed in the jet mixing region at $x/D = 10 - 18$ extending radially up to $R/D = 6$. This increase for SMC000 could be attributed to the presence of large coherent structures in the downstream region. These structures are thought to be broken for the chevron configurations due to the streamwise vortices generated by the chevron. For the installed configuration, SMC000 shows high pressure levels in the turbulence mixing region. Whereas, SMC006 shows a marginal increase compared to the SMC000 configuration

at only the sideline location. Overall, the results show that SMC006 has superior noise performance with low levels of jet installation noise and jet mixing noise at downstream locations compared to SMC000.

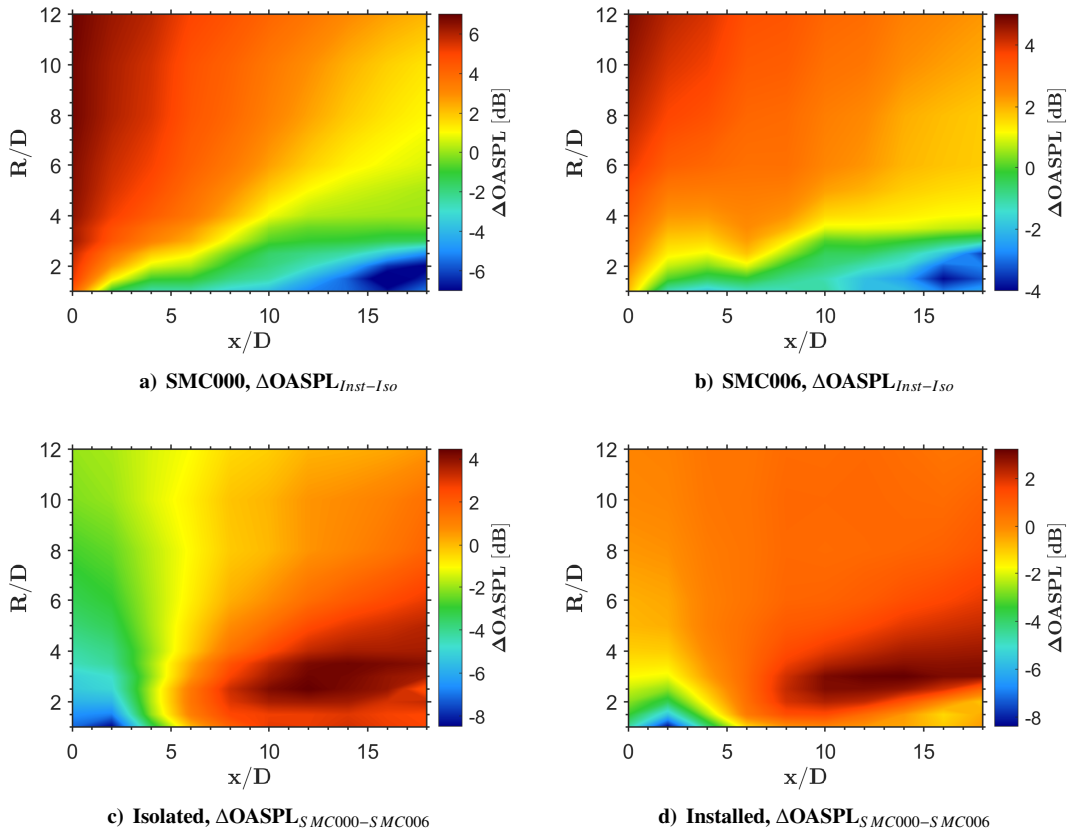

Fig. 6. Contour plots of differences in over all sound pressure level amongst the tested configurations for all the tested axial and radial positions at acoustic Mach number M = 0.5.

B. Wavelet decomposition

In order to identify the hydrodynamic and acoustic contribution of the near-field measurements, a well-established wavelet decomposition technique [21, 22] was applied. It is known from the literature that a near-field pressure signal could be considered as a combination of acoustic fluctuations and hydrodynamic contribution induced by the eddy structures. A well established WT3 method, developed by Mancinelli *et al.* [22] has been used in the present study. The pressure field along with the decomposition technique [22] is used to extract coherent structures from a vorticity field based on the procedure suggested in Ruppert-Felso *et al.* [23]. Further details about the method the readers are referred to Mancinelli *et al.* [22]. The results for the decomposed field of SMC000 and SMC006 nozzle with and without installation effect are presented in Fig. 7. The results are presented for two streamwise locations $x/D = 6$ and 12 at a radial location of $R/D = 3$, chosen based on the observations in Fig. 6. It is also important to note that $x/D = 6$ microphone is approximately positioned above the trailing edge of the flat plate. The Spectra are non-dimensionalized using Strouhal number ($St = fD/U$), where f is the frequency, U is the jet velocity and D is the diameter of the round jet.

The wavelet decomposition was carried out for isolated and installed configurations for SMC000 and SMC006 nozzles. The sound pressure level (SPL) for the original signal at axial locations $x/D = 6$ and 12 show a dominant low-frequency hump $St = 0.01 - 0.2$ as seen in Fig. 7. At location $x/D = 6$, the results for the installed configuration show a large hump at $St = 0.1 - 0.25$ compared to the isolated configuration. This hump is a characteristic feature of jet installation noise also observed in far-field noise. This hump is slightly reduced for the SMC006 nozzle compared to SMC000 (see Fig. 7a and c). At downstream location $x/D = 12$, both the isolated and installed configurations follow a similar trend over the entire spectra for SMC000. A slight reduction of up to 2 dB can be observed for the installed configuration with the absence of the characteristic hump at $St = 0.1 - 0.25$. In Fig. 7d, SMC006 installed

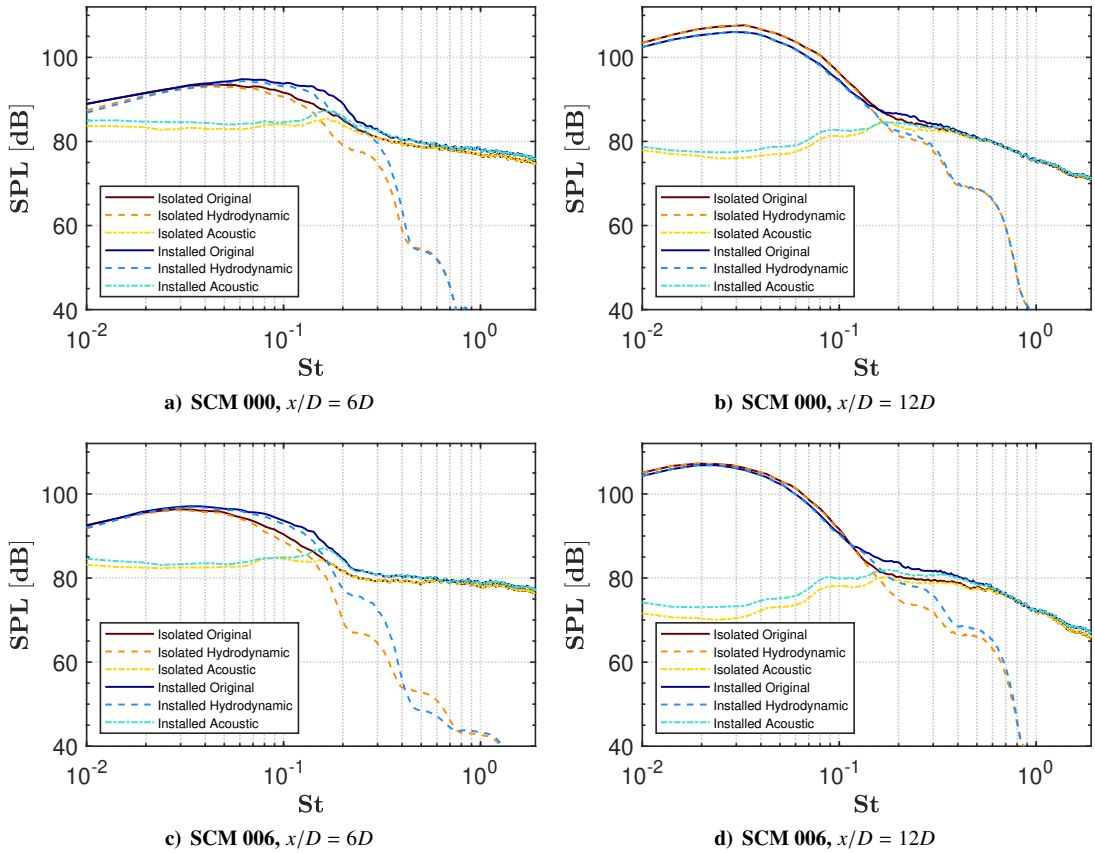

a) SCM 000, $x/D = 6D$ **b) SCM 000,** $x/D = 12D$

c) SCM 006, $x/D = 6D$ **d) SCM 006,** $x/D = 12D$

Fig. 7. Sound pressure level of the acoustic and hydrodynamic components at radial position $R/D = 3$ **for acoustic Mach number M = 0.5 for both isolated and installed jets with a plate distance of** $h/D = 2$**.**

configuration shows a marginal increase in the high frequency region $St = 0.15 - 0.5$ compared to SMC006 isolated. The contribution from the acoustic component in Fig. 7a for SMC000 shows a small hump $St = 0.1 - 0.25$ at $x/D = 6$ revealing that the increased spectral hump for the installed configuration is contributed by the acoustic part. This small hump is higher for the SMC006 installed configuration in Fig. 7c compared to the isolated from which it could be concluded that the increase in SPL for installed configuration at $St = 0.1 - 0.25$ is mostly due to acoustic scattering. Overall, the results show that the most dominant characteristic in the near-field pressure measurements is a dominant low-frequency hump $St = 0.01 - 0.2$, and it belongs to the hydrodynamic part of the jet noise sources. A marginal contribution to the spectral hump between $St = 0.1 - 0.25$ for the installed configuration is contributed by the acoustic part of the signal.

C. Hydrodynamic field investigation

Previous studies [1,24–26] have shown that the near-field pressure moving away from the jet axis in the radial direction can be divided into three regions: a nonlinear hydrodynamic field ($R/D = 0 - 1$), a linear hydrodynamic field ($R/D = 1 - 2.7$) and an acoustic field ($R/D > 2.7$) [24]. Furthermore, it is also well established that the hydrodynamic pressure fluctuations display an exponential decay in the radial direction. In order to demonstrate the hydrodynamic behaviour of the round and chevron nozzle, the SPL for the near-field pressure at different radial positions for SMC000 and SMC006 for isolated and installed configurations are presented in Fig. 8. The results for isolated jets are shown as a solid line and installed jets are shown as dashed lines with the top row showing results for SMC000 and the bottom row showing results for SMC006. At axial location $x/D = 6$, SMC000 shows a large spectral hump $St = 0.1 - 0.7$. Previous studies have shown the spectral peak region as the energy-containing region ($St = 0.1 - 0.4$), the following decay as the inertial sub-range $St = 0.4 - 0.7$ and higher frequencies as the acoustic region $St > 0.7$. SMC000 installed configuration shows a reduction of up to 2 dB compared to the installed configuration in the energy-containing and inertial sub-range. In the case of SMC006, the installed configuration has very minimal noise reduction compared to its respective isolated jet. Interestingly, outside the linear hydrodynamic field $R/D > 3$, the installation case shows a

dominant spectral hump at frequencies $St = 0.02 - 0.3$, which gets stronger at increasing radial distances. Moreover, a double hump behavior could be observed at $R/D = 10$ for both the round and chevron nozzles. In the turbulence mixing region $x/D = 12$, the spectral levels are considerably high compared to $x/D = 6$ for both the nozzles. SMC000 installed configuration shows considerable reductions in the pressure levels compared to the round isolated nozzle. In the case of SMC006 installed, the noise reduction is not as substantial. The increase in spectral hump outside the linear hydrodynamic region can also be observed at $x/D = 12$, however, the double peak behavior is absent at this axial location.

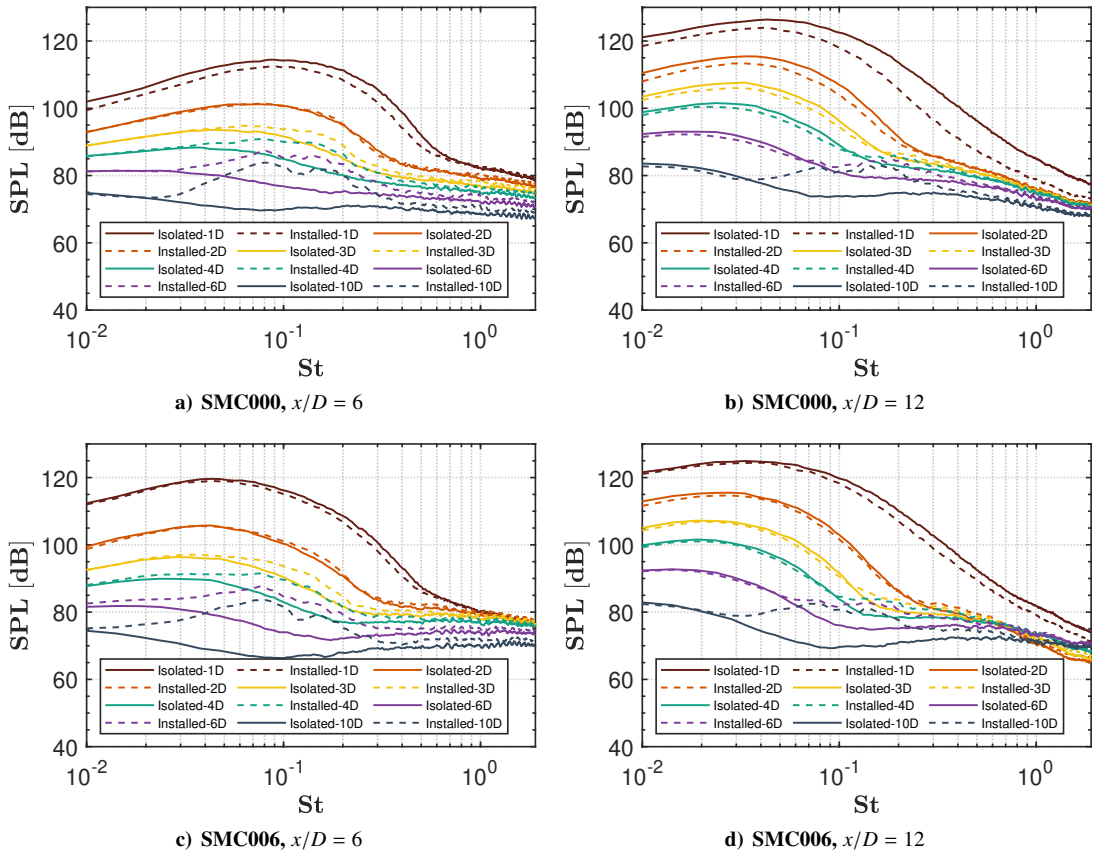

a) SMC000, $x/D = 6$ **b) SMC000,** $x/D = 12$

c) SMC006, $x/D = 6$ **d) SMC006,** $x/D = 12$

Fig. 8. Sound pressure level at several radial location (shown in legend) and at axial locations $x/D = 6$ and 12 at acoustic Mach number M = 0.5 for SMC000 and SMC006 for both isolated and installed jets.

To further investigate the spectral characteristics of the hydrodynamic field moving away from the jet axis contour plots of ΔSPL are presented in terms of radial measurement points and the normalised frequency Strouhal number in Fig. 9. Figures 9a, b, c, and d show the sound pressure level difference between installed and isolated configurations. Positive values show the contribution of the installed jet and negative values show the contribution of the isolated jet. At first glance, the results for both the round and chevron jet show very similar characteristics at both the presented axial locations. At axial location $x/D = 6$, the effect of jet installation is dominant at $St = 0.03 - 0.2$ in the acoustic region ranging from $R/D = 4 - 12$. The increase in pressure levels for the isolated jet appears to be localized at $St = 0.2 - 0.5$ within $R/D < 2$ for both the round and chevron nozzles. At downstream axial location $x/D = 12$, the installed jet shows an increase in the frequency range of $St = 0.04 - 0.3$ in the acoustic field. A characteristic double hump can be observed in far-field region $R/D = 8 - 12$ at $x/D = 12$ (see Fig. 9b). In order to evaluate the effect of installation between the SMC000 and SMC006, the difference between Fig. 9a,b and 9c,d was evaluated and presented in Fig. 9e and f respectively. The spectra in Fig. 9e show that the installation effect for SMC000 is much higher than SMC006 relative to their respective isolated cases, with a notable increase in the pressure levels over a wide frequency and radial range shown with positive values. SMC006 has increased relative pressure levels only at radial location $R/D = 6 - 9$ in the frequency range of $St = 0.01 - 0.1$ shown with negative values in Fig. 9e and f. In the fully developed region $x/D = 12$, at increasing radial distances, the increased pressure level for SMC006 gradually decreases to lower frequencies.

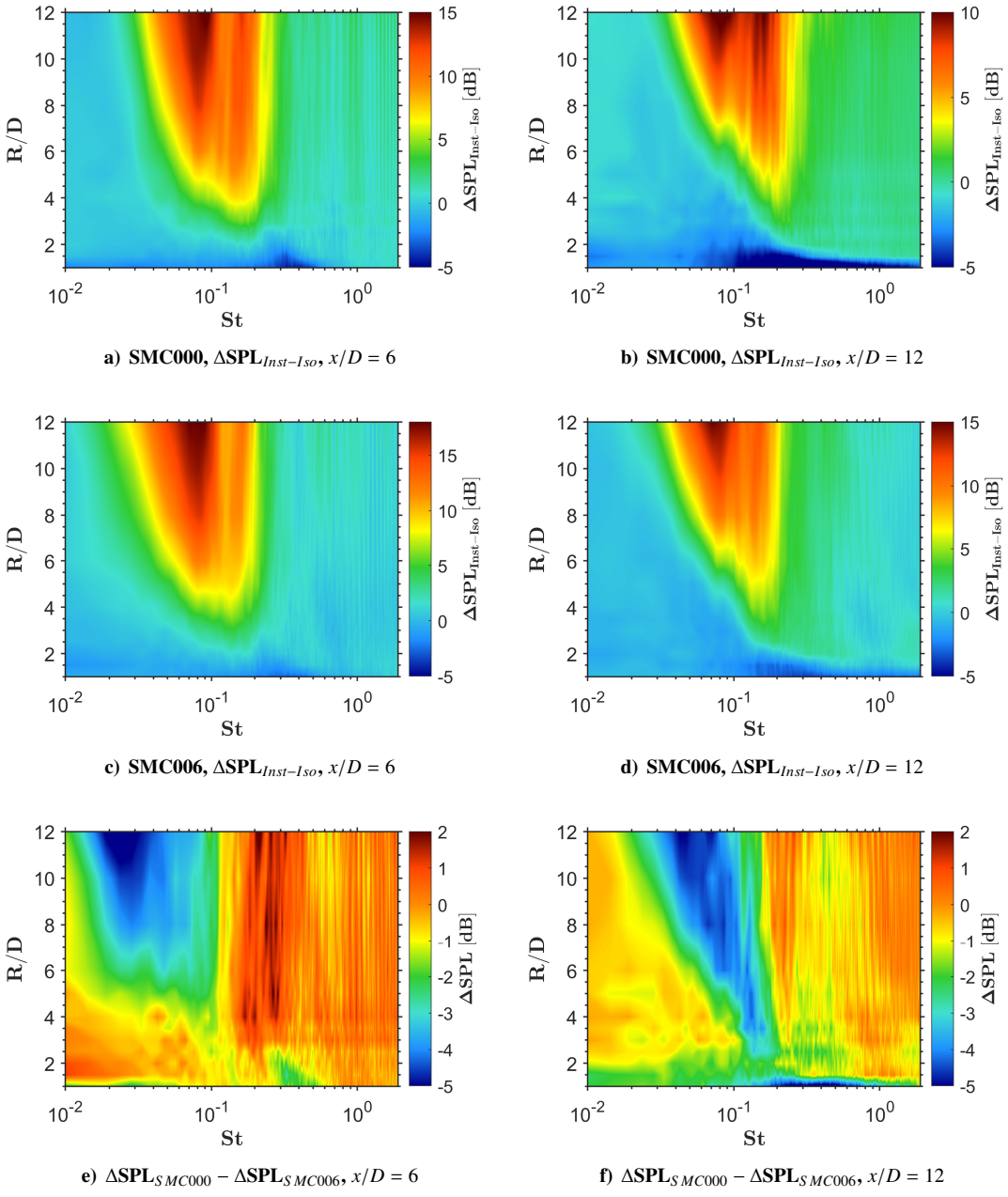

a) SMC000, $\Delta\mathbf{SPL}_{Inst-Iso}$, $x/D = 6$

b) SMC000, $\Delta\mathbf{SPL}_{Inst-Iso}$, $x/D = 12$

c) SMC006, $\Delta\mathbf{SPL}_{Inst-Iso}$, $x/D = 6$

d) SMC006, $\Delta\mathbf{SPL}_{Inst-Iso}$, $x/D = 12$

e) $\Delta\mathbf{SPL}_{SMC000} - \Delta\mathbf{SPL}_{SMC006}$, $x/D = 6$

f) $\Delta\mathbf{SPL}_{SMC000} - \Delta\mathbf{SPL}_{SMC006}$, $x/D = 12$

Fig. 9. Contours of differences in sound pressure level at various radial locations for acoustic Mach number M = 0.5 for SMC000 and SMC006 for both isolated and installed jets.

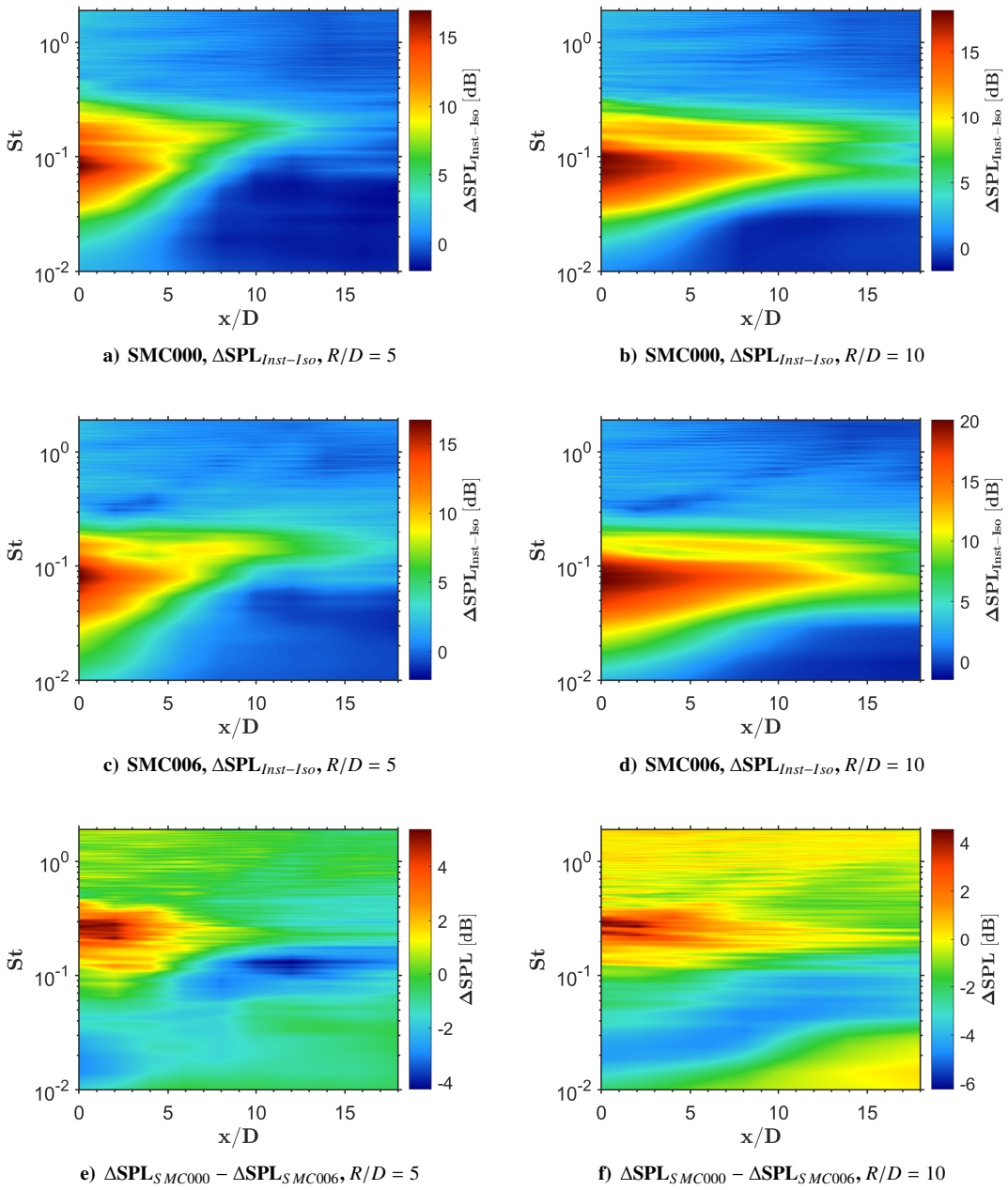

a) SMC000, ΔSPL$_{Inst-Iso}$, $R/D = 5$ **b) SMC000, ΔSPL$_{Inst-Iso}$, $R/D = 10$**

c) SMC006, ΔSPL$_{Inst-Iso}$, $R/D = 5$ **d) SMC006, ΔSPL$_{Inst-Iso}$, $R/D = 10$**

e) ΔSPL$_{SMC000} - \Delta$SPL$_{SMC006}$, $R/D = 5$ **f) ΔSPL$_{SMC000} - \Delta$SPL$_{SMC006}$, $R/D = 10$**

Fig. 10. Contours of differences in sound pressure level at radial position $R/D = 5$ and at various axial locations for acoustic Mach number M = 0.5 for SMC000 and SMC006 for both isolated and installed jets.

From Fig.9, the radial location $R/D = 5$ in the acoustic field could be identified as a region of interest as it showed the region from which the ΔSPL between the installed and isolated configurations for both SMC000 and SMC006 nozzles started to increase. Therefore, the ΔSPL between the isolated and installed configurations at $R/D = 5$ and at $R/D = 10$ was evaluated for all axial positions. The results are presented in Fig. 10 in terms of axial positions and Strouhal number with contour levels showing the difference in SPL. The ΔSPL for both the SMC000 and SMC006 show a very similar trend at both radial positions. The installed configuration shows a substantial increase in the pressure levels of up to 15 dB at $St = 0.02 - 0.3$. Increased spectral levels are observed very close to the nozzle exit, extending to the end of the potential core. SMC006 shows a marginal increase in the pressure levels at downstream locations in the low-frequency region $St < 0.1$. Interestingly, at $R/D = 10$ the two hump phenomenon often seen in jet installation noise could be seen throughout the axial positions. In order to evaluate the effect of installation between the SMC000 and SMC006, the difference between Fig. 9a,b and 9c,d was evaluated and presented in Fig. 9e and f. The results yet again show that SMC000 installed configuration has large pressure levels compared to SMC006

configuration relative to their respective isolated cases.

D. near-field correlation

The auto-correlation and cross-correlation function has been used to analyze the time scale of coherence of the near-field pressure and was computed using the following,

$$R_{p_i p_j}(\xi, \tau) = \langle p(x,t),\ p(x,t+\tau) \rangle, \tag{1}$$

where τ is the time lag and the symbol $\langle \cdot \rangle$ denotes ensemble average. The correlation coefficient $R_{p_i p_j}$ is obtained by normalizing the correlation function by the signal variance. The correlation coefficients indicate the similarity of the signals p_i and p_j at a given delay τ. The term $p_j = p_i$ when calculating the auto-correlation.

The results for the auto-correlation of the isolated and installed configurations are shown in Fig. 11a and b, respectively. The auto-correlation profile determines the characteristics of the time variation of the near-field pressure with axial distance. A direct relationship with the flow fluctuations inside the jet could be made with the near-field pressure. Therefore, near-field pressure waves propagating at various axial locations parallel to jet flow could be assessed from Fig. 11. The shape of the auto-correlation profile for SMC000 isolated is narrow without any negative peaks at the vicinity of the nozzle exit at $x/D = 2$ and gradually increases in width with slight negative peaks at downstream locations $x/D = 6$ and 10. The gradual increase in the profile could be attributed to the evolution from uncorrelated random small scale structures near the nozzle exit plane to the coherent large scale structures aft of the potential core. Comparatively, the profile for the SMC006 isolated configuration in Fig. 11a shows a narrower profile at $x/D = 2$ and a wider profile for the remaining axial locations. For installed configuration, at $x/D = 2$ shows a larger negative peak for SMC000 compared to SMC006. Moreover, the auto-correlation profile is much narrower for SMC000, which shows that the SMC006 has much finer structures compared to SMC000 and the effect of jet installation influences it very minimally.

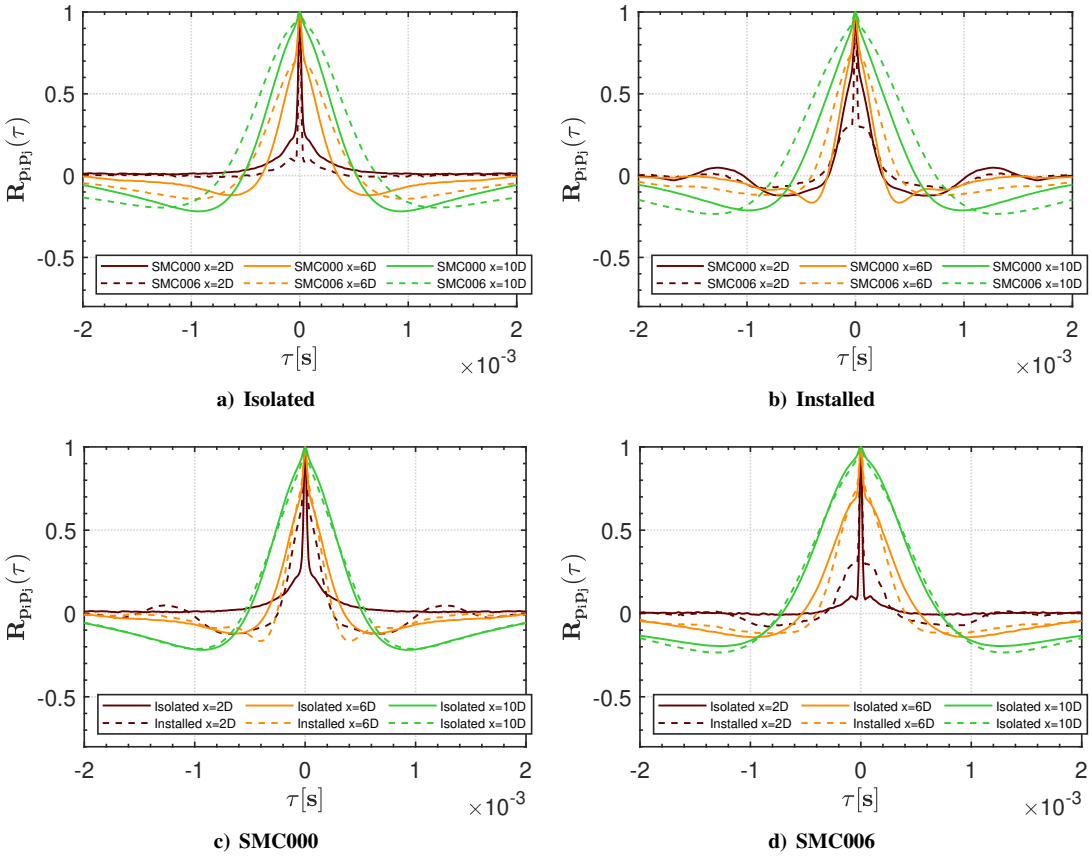

Fig. 11. Auto-correlation of the near-field measurements at acoustic Mach number M = 0.5 for SMC000 and SMC006 for both isolated and installed jets

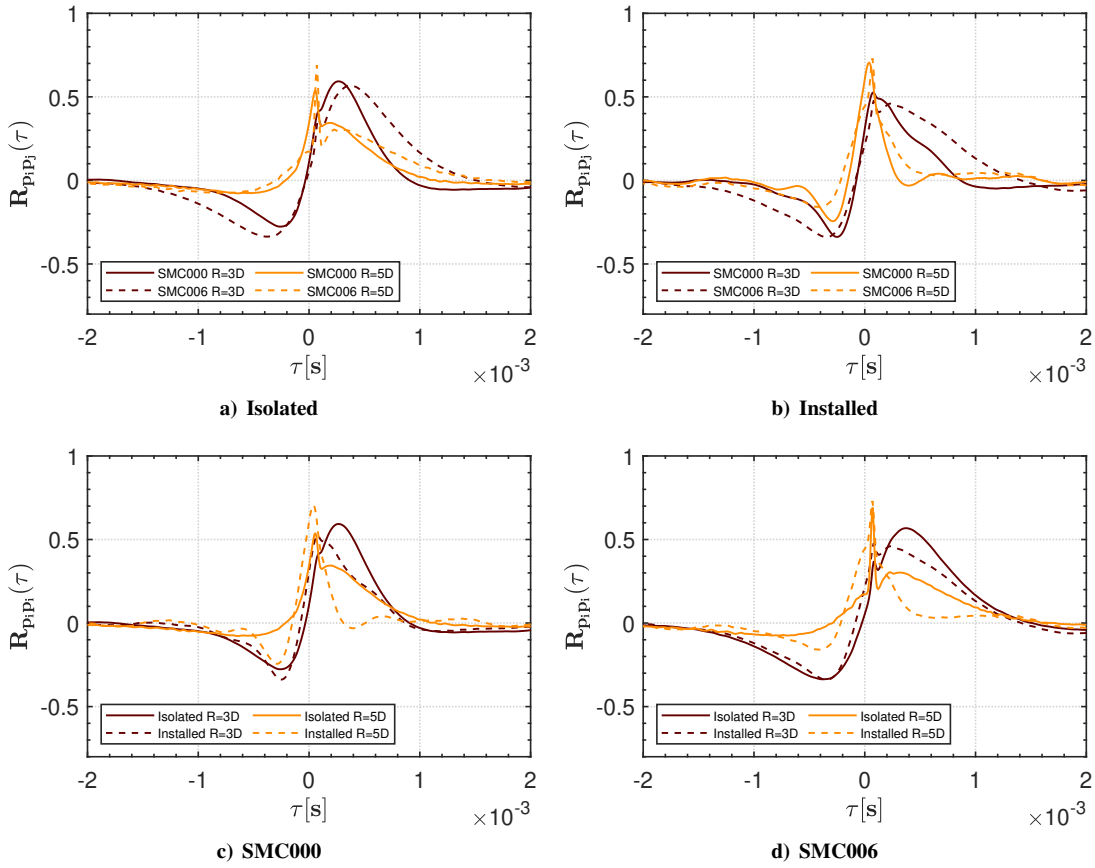

Fig. 12. Cross-correlation of the near-field pressure fluctuations between $x/D = 6$ and $x/D = 8$ at acoustic Mach number M = 0.5 for SMC000 and SMC006 for both isolated and installed jets

A comparison of the auto-correlation profiles of installed and isolated configurations is presented in Fig. 11c. For the SMC000 configuration, at nozzle exit $x/D = 2$, the profile is wider for the installed configuration with a large negative peak. Whereas in the case of SMC006, the negative peak and the width increase is minimal as seen in Fig. 11d. Overall, the profiles do not change significantly between the isolated and installed configuration at $x/D = 10$ for both the SMC000 and SMC006 nozzles.

Cross-correlation was calculated for two consecutive pressure signals acquired simultaneously from the near-field microphones for both the isolated and installed configurations. The Time delay (τ) between two pressure signals was estimated from the time difference between the peak cross-correlation coefficient of the reference ($x/D = 6$) and correlated signal $x/D = 8$. The time delay could be used to estimate the wave propagation $U_c = dx/\tau$, where dx and Uc are microphone separation distance and convective speed of the coherent signal that passes from the reference microphone to the correlated microphone. The area of investigation was chosen to be for the flow past the trailing edge. The results for the cross-correlation between $x/D = 6$ and 8 are presented for radial distances $R/D = 3$ and 5 in Fig. 12. The cross-correlation peak shows a time delay contrary to the auto-correlation results where the peak has no time delay. At first glance, the results at $R/D = 3$ have a larger hump due to the hydrodynamic field compared to $R/D = 5$ where the field is acoustic with a much sharper cross-correlation profile. When considering the isolated jet, SMC000 has a smaller time delay compared to the SMC006 at both the presented radial positions as seen in Fig. 12. For the installed configuration a similar trend is followed with SMC000 having a smaller time delay.

IV. Conclusion

An experimental investigation of the hydrodynamic field of cold jets was carried out at the BJARF facility at the University of Bristol. One round nozzle and four types of chevron nozzles were investigated in an isolated and installed configuration for a wide range of Mach numbers. The measurements were carried out using a linear array of 10 microphones distributed axially at a distance of 2D ranging from $x/D = 0 - 18$. The microphone array was traversed to 12 positions radially ranging from $R/D = 1 - 12$. The OASPL results for axially placed microphones

showed that chevrons lead to an increase in OASPL in the initial region and a possible reduction in the pressure levels in the intermediate and fully developed region. SMC006 nozzle with increased penetration angle showed the best performance in terms of reduction in pressure levels. Contour maps of OASPL for round and the best performing chevron nozzle showed that the isolated jet possesses high-pressure levels in the fully developed region compared to the installed jets. Installed jets have increased pressure levels in the jet sideline mostly outside the linear hydrodynamic region in the acoustic field. Comparing the round and chevron nozzles, isolated chevron nozzles show an increase in pressure levels in the vicinity of the jet in the sideline region. Whereas the round nozzle shows a substantial increase in the fully developed region compared to the chevron nozzle in both the isolated and installed configurations. A well-established wavelet decomposition method was used to investigate the near-field pressure to know the nature of the jet noise sources. The outcome showed that energy containing spectral hump ($St = 0.01 - 0.2$) was generated due to the hydrodynamic field. In the case of installed configuration, a small increase ($St = 0.15 - 0.2$) in the energy containing spectral hump was found, and the outcome of the analysis identified the increase to be due to the acoustic part of the decomposed signal. The use of chevrons showed a reduction in the spectral hump ($St = 0.15 - 0.2$) but retained the smaller hump caused by the acoustic part. Near-field pressure was investigated to characterize its effect at a different radial distance. The sound pressure level of the installed configuration showed a reduction in the linear hydrodynamic region compared to the isolated configuration. However, in the acoustic field, $R/D > 3$ the installed configuration showed a considerable increase compared to the isolated configuration. Spectral plots of radial distances vs frequency in terms of SPL differences at $x/D = 6$ showed a substantial increase in the pressure levels for the installed configuration in the acoustic field ranging from $R/D = 3 - 10$ after which the energy appears to have reduced. These were observed in both the round and chevron nozzle, a comparison of the SPL differences between the nozzles showed a substantial increase in the SPL levels over a wide frequency range and radial distances for the round nozzle. A select radial distance was chosen ($R/D = 5$) and the spectral plot of axial distances vs frequency was investigated. The outcome of which showed that SPL differences for the installed configuration are higher close to the nozzle exit and high levels of pressure are found between $x/D = 0 - 5$. A comparison of the SPL difference between the two nozzles yet again showed high levels of a relative pressure difference for the round nozzle between the isolated and installed configurations. Analysis of the near-field auto-correlation showed a wider profile for chevrons compared to the round nozzle at the intermediate region. Close to the nozzle exit chevron nozzle showed a narrower profile compared to the round nozzle. Narrow peaks could be related to uncorrelated random structures and a wider profile could be attributed to the coherent large-scale structures. Cross-correlation showed a shorter time delay for round jet compared to chevron for both isolated and installed configurations. Overall, the near-field pressure fluctuations have shown that chevrons provide a considerable amount of noise reduction compared to round jet in both the isolated and installed configurations.

Acknowledgement

The authors would like to acknowledge the Engineering and Physical Sciences Research Council (EPSRC) for supporting this research titled JINA: Jet Installation Noise Abatement (Grant No. EP/S000917/1).

References

[1] Rego, L., Avallone, F., Ragni, D., and Casalino, D., "Jet-installation noise and near-field characteristics of jet–surface interaction," *Journal of Fluid Mechanics*, Vol. 895, 2020.

[2] Brown, W. and Ahuja, K., "Jet and wing/flap interaction noise," *9th Aeroacoustics Conference*, 1984, p. 2362.

[3] Cavalieri, A. V., Jordan, P., Wolf, W. R., and Gervais, Y., "Scattering of wavepackets by a flat plate in the vicinity of a turbulent jet," *Journal of sound and Vibration*, Vol. 333, No. 24, 2014, pp. 6516–6531.

[4] Thomas, R. H., Mengle, V. G., Brunsniak, L., and Elkoby, R., "Reducing Propulsion Airframe Aeroacoustic Interactions With Uniquely Tailored Chevrons: 3. Jet-Flap Interaction," 2006.

[5] Belyaev, I. V., Faranosov, G. A., Ostrikov, N. N., and Paranin, G., "A parametric experimental study of jet-flap interaction noise for a realistic small-scale swept wing model," *21st AIAA/CEAS Aeroacoustics Conference*, 2015, p. 2690.

[6] Markesteijn, A. P. and Karabasov, S. A., "GPU CABARET Flow and Noise Solutions of an Installed Jet Configuration," *AIAA AVIATION 2020 FORUM*, 2020, p. 2563.

[7] Lawrence, J., Azarpeyvand, M., and Self, R., "Interaction between a flat plate and a circular subsonic jet," *17th AIAA/CEAS Aeroacoustics Conference (32nd AIAA Aeroacoustics Conference)*, 2011, p. 2745.

[8] Brown, C. A., "Jet-surface interaction test: far-field noise results," *Journal of Engineering for Gas Turbines and Power*, Vol. 135, No. 7, 2013.

[9] Papamoschou, D., "Prediction of jet noise shielding," *48th AIAA Aerospace Sciences Meeting Including the New Horizons Forum and Aerospace Exposition*, 2010, p. 653.

[10] Lawrence, J., *Aeroacoustic interactions of installed subsonic round jets*, Ph.D. thesis, University of Southampton, 2014.

[11] Podboy, G. G., *Jet-Surface interaction test: phased array noise source localization results*, Vol. 44670, American Society of Mechanical Engineers, 2012.

[12] Tam, C. K. and Chandramouli, S., "Jet-plate interaction tones relevant to over-the-wing engine mount concept," *Journal of Sound and Vibration*, 2020, pp. 115378.

[13] Bridges, J. and Brown, C., "Parametric testing of chevrons on single flow hot jets," *10th AIAA/CEAS aeroacoustics conference*, 2004, p. 2824.

[14] Massey, S., Elmiligui, A., Hunter, C., Thomas, R., Pao, P., and Mengle, V., "Computational Analysis of a Chevron Nozzle Uniquely Tailored for Propulsion Airframe Aeroacoustics," 05 2006.

[15] Kamliya Jawahar, H., Markesteijn, A. P., Karabasov, S. A., and Azarpeyvand, M., "Effects of Chevrons on Jet-installation Noise," *AIAA AVIATION 2021 FORUM*, 2021, p. 2184.

[16] Kamliya Jawahar, H., Baskaran, K., and Azarpeyvand, M., "Unsteady Characteristics of Mode Oscillation for Screeching Jets," *AIAA AVIATION 2021 FORUM*, 2021, p. 2279.

[17] Kamliya Jawahar, H., Meloni, S., Camussi, R., and Azarpeyvand, M., "Experimental Investigation on the Jet Noise Sources for Chevron Nozzles in Under-expanded Condition," *AIAA AVIATION 2021 FORUM*, 2021, p. 2181.

[18] Kamliya Jawahar, H. and Azarpeyvand, M., "Trailing-edge Treatments for Jet-installation Noise Reduction," *AIAA AVIATION 2021 FORUM*, 2021, p. 2185.

[19] Meloni, S. and Kamliya Jawahar, H., "A Wavelet-Based Time-Frequency Analysis on the Supersonic Jet Noise Features with Chevrons," *Fluids*, Vol. 7, No. 3, 2022, pp. 108.

[20] Mayer, Y. D., Jawahar, H. K., Szőke, M., Ali, S. A. S., and Azarpeyvand, M., "Design and performance of an aeroacoustic wind tunnel facility at the University of Bristol," *Applied Acoustics*, Vol. 155, 2019, pp. 358–370.

[21] Grizzi, S. and Camussi, R., "Wavelet analysis of near-field pressure fluctuations generated by a subsonic jet," *Journal of Fluid Mechanics*, Vol. 698, 2012, pp. 93.

[22] Mancinelli, M., Pagliaroli, T., Di Marco, A., Camussi, R., and Castelain, T., "Wavelet decomposition of hydrodynamic and acoustic pressures in the near field of the jet," *Journal of Fluid Mechanics*, Vol. 813, 2017, pp. 716.

[23] Ruppert-Felsot, J., Farge, M., and Petitjeans, P., "Wavelet tools to study intermittency: application to vortex bursting," *Journal of Fluid Mechanics*, Vol. 636, 2009, pp. 427–453.

[24] Arndt, R. E., Long, D., and Glauser, M., "The proper orthogonal decomposition of pressure fluctuations surrounding a turbulent jet," *Journal of Fluid Mechanics*, Vol. 340, 1997, pp. 1–33.

[25] Suzuki, T. and Colonius, T., "Instability waves in a subsonic round jet detected using a near-field phased microphone array," *Journal of Fluid Mechanics*, Vol. 565, 2006, pp. 197–226.

[26] Tinney, C. and Jordan, P., "The near pressure field of co-axial subsonic jets," *Journal of Fluid Mechanics*, Vol. 611, 2008, pp. 175–204.